Disconnected Glass-Glass Transitions and Diffusion Anomalies in a model with two repulsive length scales

Matthias Sperl
Institut für Materialphysik im Weltraum, Deutsches Zentrum für Luft- und Raumfahrt, 51170 Köln, Germany

Emanuela Zaccarelli and Francesco Sciortino
Dipartimento di Fisica and CNR-INFM-SOFT, Universita' di Roma La Sapienza, Piazzale A. Moro 2, 00185 Roma, Italy

Pradeep Kumar
Center for Studies in Physics and Biology, Rockefeller University, New York, NY 10021, USA

H. Eugene Stanley
Department of Physics and Center for Polymer Studies, Boston University, Boston, Massachusetts 02215, USA

(Dated: October 19, 2009)

Building on mode-coupling-theory calculations, we report a novel scenario for multiple glass transitions in a purely repulsive spherical potential: the square-shoulder. The liquid-glass transition lines exhibit both melting by cooling and melting by compression as well as associated diffusion anomalies, similar to the ones observed in water. Differently from all previously investigated models, here for small shoulder widths a glass-glass line is found that is disconnected from the liquid phase. Upon increasing the shoulder width such a glass-glass line merges with the liquid-glass transition lines, featuring two distinct endpoint singularities that give rise to logarithmic decays in the dynamics. These findings can be explained analytically by the interplay of different repulsive length scales.

PACS numbers: 64.70.Q-, 66.30.jj, 64.70.ph, 64.70.pe

In the field of glassy slow dynamics, many experiments and simulations have been inspired in recent years by the mode-coupling theory of the glass transition (MCT) [1]. The theory deals with density autocorrelation functions $\phi_q(t)$ with wave vectors q, and predicts their long-time limits f_q. While in the liquid state $f_q = 0$, the glass state is defined by $f_q > 0$. MCT was first applied to the hard-sphere system (HSS) where a liquid-glass transition was identified [2], and confirmed by experiments [3]. In addition to liquid-glass transitions, for certain interactions MCT also predicts glass-glass transitions: In this case an existing first glass state with f_q^1 transforms into a second distinct glass state with $f_q^2 > f_q^1$ discontinuously. Such glass-glass transitions were predicted for the square-well system (SWS) where the hard-core repulsion is supplemented by a short-ranged attraction [4, 5, 6]. In the SWS, the first glass state is driven by repulsion like in the HSS and the second glass state is driven by attraction. The competition between these two mechanisms is responsible for the emergence of glass-glass transitions. Such a line of glass-glass transitions extends smoothly a line of liquid-glass transitions into the glass state and terminates in an endpoint singularity. Close to the endpoint singularity the dynamics is ruled by logarithmic relaxation [7]. The predicted logarithmic decays were identified in computer simulations and establish the relevance of endpoint singularities for the description of glassy dynamics [8, 9]. A second dynamical anomaly predicted for the SWS concerns a reentrant liquid-glass line that causes melting by cooling [4, 5, 6]. This prediction of MCT was confirmed by computer simulation [10] and by experiments in colloidal suspensions [11, 12].

In this work we replace the attractive length scale in the SWS by a second repulsive length scale δ of the square-shoulder system (SSS) as shown in Fig. 1. The SSS can be considered the simplest potential with two competing interparticle distances; it is applied to describe properties of metallic glasses like cerium or cesium [13], micellar [14] and granular materials [15], silica [16] and water [17].

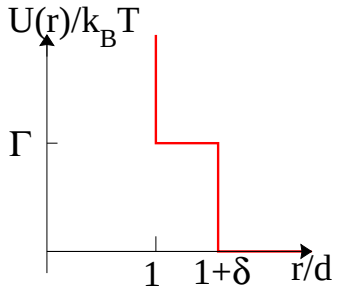

FIG. 1: Square-shoulder potential with control parameters packing fraction $\varphi = \pi\rho d^3/6$, shoulder height $\Gamma = u_0/k_B T$, and shoulder width δ for particles of diameter d at density ρ.

In the following, the glass-transition diagrams are calculated from the singularities of the MCT functional [1]

$$\mathcal{F}_q[\mathbf{V}, f_k] = \sum_{\vec{k}+\vec{p}=\vec{q}} V_{q,kp}\, f_k f_p = \frac{f_q}{1-f_q}\,, \qquad (1a)$$

with vertex $\mathbf{V}$ given by wave vector moduli q, k, p, the static

structure factor S_q, and the direct correlation function c_q:

$$\sum_{\vec{k}+\vec{p}=\vec{q}} V_{q,k\,p}\, f_k f_p,\; V_{q,k\,p} = \rho S_q S_k S_p \{\vec{q}\cdot[\vec{k}\,c_k + \vec{p}\,c_p]\}^2/q^4. \quad \text{(1b)}$$

Quantities S_q and c_q are given by the interaction potential. The discretization of the functionals is chosen like for the HSS and the SWS [5, 18] with a number of wave vectors $M = 600$ and a wave-vector cutoff $dq_{\max} = 80$, the static structure factors of the SSS are obtained within the Rogers-Young (RY) approximation [19, 20]; further details of the calculations shall be found in a subsequent publication [21]. For specific values of the control parameters packing fraction φ, shoulder height Γ, and shoulder width δ, Eq. (1) exhibits singularities where the f_q change discontinuously indicating liquid-glass or glass-glass transitions. At these singularities one can define the so-called exponent parameter $\lambda < 1$ that fixes all other critical exponents of the theory [1]. While typically at liquid-glass transitions, $\lambda \approx 0.7$, λ approaches unity at the endpoint of glass-glass transition lines signaling the emergence of logarithmic decay laws [7].

Figure 2(a) shows the glass-transition scenario for $\delta = 0.13$: The liquid-glass transition line (diamonds) starts at the HSS limiting value of $\varphi^c_{\rm HSS} = 0.5206$ (dotted line for small Γ) for vanishing shoulder width Γ. For increasing shoulders and up to $\Gamma \approx 1.5$, the curve exhibits a shift in the transition packing fraction $\varphi(\Gamma)$ to higher values – the glass initially melts upon cooling. This trend can be traced to the evolution of the static structure factor which becomes sharper and moves to lower wave vectors for higher Γ; the corresponding pair distribution functions show a higher probability for particles being at larger distances from each other. Hence, larger particle separations weaken the cage and are compensated by higher densities at the glass transition, cf. [21] for more details and a comparison to the melting-by-cooling phenomenon in the SWS. For shoulder heights from $2k_BT$ to $3.5k_BT$, i.e. for $2 \lesssim \Gamma \lesssim 3.5$, the glass-transition curve bends downwards and reaches the limiting value of the HSS for the outer core $\hat{\varphi}^c_{\rm HSS} = \varphi^c_{\rm HSS}/(1+\delta)^3 = 0.3608$ (dotted line for large Γ).

If the packing fractions and repulsive strengths are increased beyond the liquid-glass transition line, one encounters an additional line of glass-glass-transition singularities (filled circles). Differently from glass-glass lines in all models investigated previously, this additional line is located inside the glassy regime, disconnected from any liquid-glass transition line. It is bounded by two endpoint singularities (open circles) where the additional discontinuity in the f_q vanishes, λ reaches unity, and logarithmic decay laws emerge.

When increasing the shoulder width δ further, the glass-glass and liquid-glass transition lines move towards each other and start to merge for sufficiently high shoulders at around $\delta = 0.145$. Figure 2(b) shows the situation for $\delta = 0.15$: From $\Gamma = 2.0$ to 3.5, the former glass-glass line now indicates a transition from the liquid directly into the second glass state. For $\Gamma < 2.0$ and for $\Gamma > 3.5$, the formerly isolated glass-glass line crosses the liquid-glass line and extends into the glassy regime

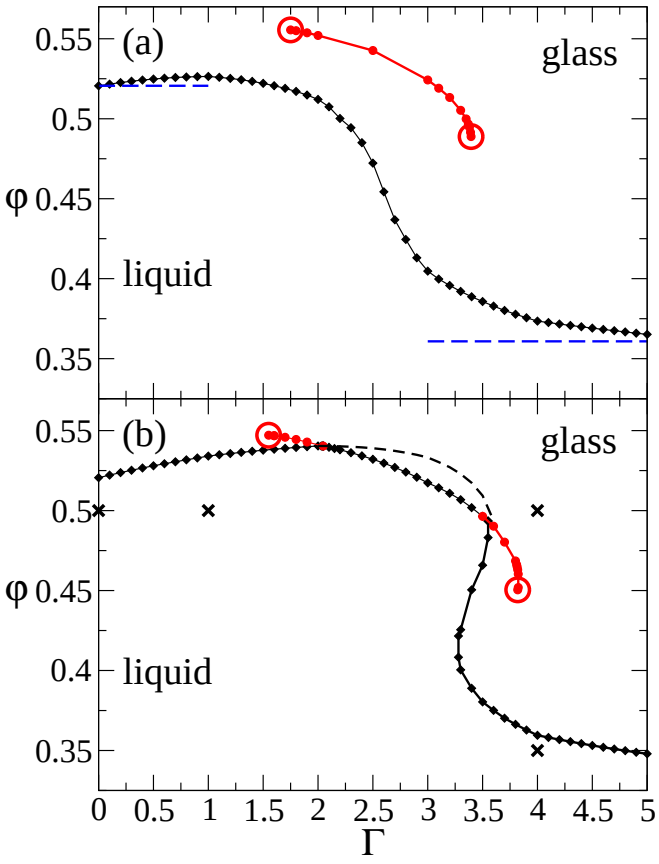

FIG. 2: Glass-transition diagrams for the SSS. Diamonds (♦) indicate liquid-glass transitions, filled circles (●) show glass-glass transition points terminating in two endpoint singularities (○). (a) $\delta = 0.13$. Dashed lines display the respective limits for hard spheres of diameter 1 and $1+\delta$. The line of glass-glass transitions is disconnected from the line of liquid-glass transitions, and moves towards and crosses it for larger shoulder width. (b) $\delta = 0.15$. Crosses (×) indicate the four states discussed in Fig. 3 relating the glass-glass transitions to features in the static structure. The dashed curve exhibits the liquid-glass transition line for a reduced wave-vector cutoff of $dq_{\max} = 40$ demonstrating that without contributions of higher wave vectors to the functional in Eq. (1) the lines of glass-glass transitions are absent.

as two glass-glass transition lines. On both ends, the endpoint singularities retreat individually in a generic way which is similar to the case of the SWS [5].

Figure 2(b) also exhibits the reentry phenomenon melting-by cooling for small Γ as discussed before for $\delta = 0.13$, but in addition a second reentry phenomenon is found between $\Gamma = 3.0$ and 3.5 where melting can also be induced by compression. The trends can again be traced back to the behavior of the static structure [21]: Increasing the packing fraction from low values to around $\varphi \approx 0.45$, the pair distribution function shows an increased probability for particle contact at both inner and outer cores. However, for values larger than $\varphi \approx 0.45$, the contact at the inner core grows at the expense of contact at the outer core; interparticle contacts at the outer core are suppressed by the high density and particles now col-

lide much more frequently at their inner cores. Since the cage represented by the inner core is too loose to trigger glassy arrest at such density, this is compensated by lower temperature (or equivalently by higher Γ) at the glass transition.

For the SSS, the interplay between the hard and the soft core is manifest in changes at the (1) principal peaks signaling different interparticle distances, and (2) by a beating at larger wave vectors that is introduced by the oscillation frequencies q and $(1+\delta)q$, respectively. As explained above, changes in the principal peaks are sufficient to understand the overall behavior of the liquid-glass transition lines, including both reentry phenomena. In the following we demonstrate that mechanism (2) is responsible for the glass-glass transitions.

It is known from the theory of Fourier transformations that the discontinuities of the direct correlation function in space, $c(r)$, determine the large-wave-vector behavior of the direct correlation function c_q which enters the MCT functional in Eq. (1b) [22]. For the square-shoulder potential the dominant singularities are inner and outer core which in leading order may be modeled by two independent hard-sphere diameters. To obtain a qualitative picture, regardless of the specific form of the closure relation, it is enough to consider HSS in Percus-Yevick (PY) approximation for which c_q is known analytically [23]. For large enough wave vectors its asymptotic behavior $c_q^{\rm asy}$, reads

$$c_q^{\rm asy} = B(\varphi)\frac{\cos(q)}{q^2} = \frac{1+\varphi/2}{(1-\varphi)^2}\frac{4\pi}{q^2}\cos(q)\,. \qquad (2)$$

$c_1^{\rm asy}(q)$ for the inner core and $c_2^{\rm asy}(q)$ for the outer core are then given by $c_1^{\rm asy}(q) = B_1\cos(q)/q^2$ and $c_2(q) = B_2\cos(q[1+\delta])/q^2$, where factors of $(1+\delta)$ in q^2 were absorbed into B_2. This analytical PY result for the asymptotic decay describes the numerical solution of the RY structure factor very accurately as seen in the upper panel of Fig. 3. While for the respective limits of small and large hard spheres, $c_1^{\rm asy}(q)$ and $c_2^{\rm asy}(q)$, are relevant only individually, for parameters in between, one expects an additive effect from both cores. Assuming the PY result for both cores we get for the combination $c^{\rm asy}(q) = c_1^{\rm asy}(q) + c_2^{\rm asy}(q)$:

$$\begin{aligned} c(q)^{\rm asy} &= \tfrac{1}{q^2}\{2B_2\cos([1+\delta/2]q)\cos(q\delta/2) \\ &\quad +(B_1-B_2)\cos(q)\} \\ &= \tfrac{1}{q^2}\{2B_1\cos([1+\delta/2]q)\cos(q\delta/2) \\ &\quad +(B_2-B_1)\cos([1+\delta]q)\} \end{aligned} \qquad (3)$$

For $B_1 = B_2$, the second lines in Eq. (3) vanish and a simple beating is obtained, for $B_1 \neq B_2$ additional terms remain. Figure 3 demonstrates the evolution of the tail in c_q for increasing shoulder height. Starting from the HSS of the inner core (upper panel of Fig. 3), we get the original $1/q^2$ decay as inferred from Eq. (2) or equivalently the second line in Eq. (3). Switching on the shoulder, $B_1 > B_2 > 0$, the original tail is lowered to $B_1 - B_2$ and an additional modulation of Δq is obtained for the term with mixed frequency. For the amplitude variation of the beating one obtains $d\Delta q = 2\pi/\delta$, so for $\delta = 0.15$ one

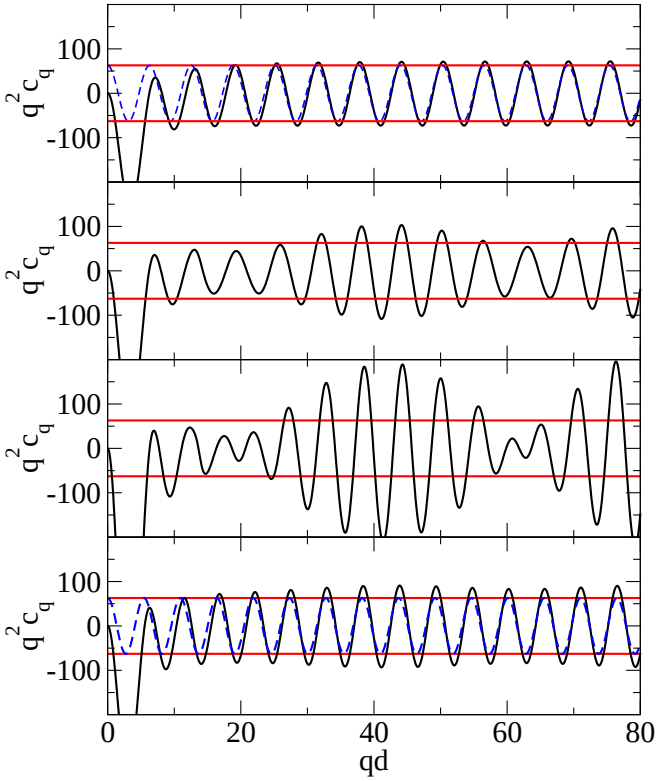

FIG. 3: Direct correlation function q^2c_q for $\delta = 0.15$, $\varphi = 0.50$, and $\Gamma = 0.0$, 1.0, and 4.0, respectively from top, $\Gamma = 4.0$ and $\varphi = 0.35$ in the bottom panel, cf. crosses in Fig. 2(b). Full horizontal lines display the value of $B(\varphi)$ in Eq. (2) for $\varphi = 0.50$. The dashed curve in the upper panel shows the asymptotic solution of Eq. (2), the dashed curve in the bottom panel shows the asymptotic solution of Eq. (2) with q replaced by $(1+\delta)q$. The emergence and vanishing of a beating from top to bottom explains the occurrence of the glass-glass transition lines in Figs. 2(a) and 2(b) through additional contributions to the functional in Eq. (1).

gets $\Delta q \approx 42d^{-1}$, a beating of amplitude variation of $qd \approx 42$ as seen in Fig. 3 in the two middle panels. If both diameters are of equal importance, the beating terms in the first lines of Eq. (3) become dominant as seen in the third panel of Fig. 3. If the outer core is dominant, the second equation in Eq. (3) is relevant: Now the decay for the larger core is supplemented by the same beating but with prefactor B_1. For yet higher contributions from the outer core the beating vanishes again as is seen in the bottom panel of Fig. 3.

Figure 3 explains the origin of the glass-glass transition line by the evolution of additional contributions to the MCT vertex in Eq. (1b). While the upper panel shows a tail in c_q that is small enough to no longer influence the MCT vertex, the subsequent panels show contributions to the integrals from the beating at wave vectors from $qd = 20$ to 80 that cannot be neglected. To show that it is these contributions that cause the glass-glass transition line we eliminate these contributions by shifting the wave-vector cutoff from $qd = 80$ to $qd = 40$ and perform additional calculations. The result is shown in Fig. 2(b) as the dashed line. With the beating switched off,

the dashed line of liquid-glass transitions is recovered without any indication of crossings or glass-glass transitions. Figure 3 also demonstrates that the beating is only relevant in a finite region that is bound from above and from below which relates to both endpoints of the glass-glass transition line.

To make contact with experimental systems, we redraw the transition diagram of Fig. 2(b) in a pressure-vs-temperature, P-T, diagram in Fig. 4, using the RY thermodynamically consistent equation of state. For a path of constant T and variable P, the diffusivity of the dynamics varies with the distance from the liquid-glass transition line. E. g., for $T \approx 0.35 u_0/k_B$ and starting from low P, the diffusivity first decreases until $P \approx 15 u_0/d^3$, then it increases anomalously until around $P \approx 30 u_0/d^3$, and then it decreases again. Such behavior, known as diffusion anomaly, is experimentally observed in liquid water [24].

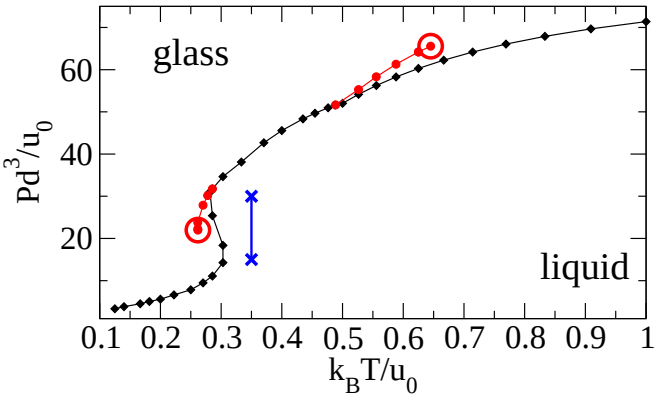

FIG. 4: Data from Fig. 2(b) for $\delta = 0.15$ shown with variables pressure P and temperature T. Crosses ($\times$) delimit the approximate region for a diffusion anomaly. Above and below that region, the diffusion coefficient decreases with pressure – within the region the diffusion coefficient increases with pressure P.

In conclusion, MCT calculations predict that the square-shoulder system is characterized by an unusual slow dynamics, based on the competition between two repulsive length scales. This manifests itself in an unexpected glass-glass transition line which can be completely disconnected from the liquid phase. Upon reducing the distance between the two repulsive lengths, the glass-glass transition line moves towards the glass-liquid line, merging for a special value of the shoulder width and giving rise to logarithmic behavior of the decay of correlations in a wide region of temperatures and densities. The mechanism for the glass-glass transitions is derived analytically from features of the static structure factor: The two length scales are reflected in a beating at large wave vectors in S_q that cause additional contributions to the MCT functional and thus trigger an extra transition.

The peculiar shape of the arrest lines echoes also in the liquid phase, generating diffusion anomalies (i.e. non monotonic dependence of the diffusion coefficient with the control parameter, either T, φ or P). The relevance of the glass-glass transition scenario found here goes beyond the specific SSS potential: The competition between two repulsive length scales and the presence of diffusion anomalies are observed in several different contexts, ranging from soft matter systems [14, 25] to silica [16], and complex liquids [26, 27, 28]. Our work opens a perspective for understanding slow dynamics in these disparate systems.

We thank W. Götze, J. Horbach, A. Meyer and P. Ziherl for fruitful discussions. MS acknowledges support from DFG Sp714/3-1 and BMWi 50WM0741. EZ and FS acknowledge support from ERC-226207-PATCHYCOLLOIDS. PK and HES thank NSF Chemistry Division for support.

[1] W. Götze, *Complex Dynamics of Glass-Forming Liquids: A Mode-Coupling Theory* (Oxford University Press, Oxford, 2009).
[2] U. Bengtzelius, W. Götze, and A. Sjölander, J. Phys. C **17**, 5915 (1984).
[3] W. van Megen and P. N. Pusey, Phys. Rev. A **43**, 5429 (1991).
[4] J. Bergenholtz and M. Fuchs, Phys. Rev. E **59**, 5706 (1999).
[5] K. Dawson, G. Foffi, M. Fuchs, W. Götze, F. Sciortino, M. Sperl, P. Tartaglia, T. Voigtmann, and E. Zaccarelli, Phys. Rev. E **63**, 011401 (2000).
[6] L. Fabbian, W. Götze, F. Sciortino, P. Tartaglia, and F. Thiery, Phys. Rev. E **59**, R1347 (1999).
[7] W. Götze and M. Sperl, Phys. Rev. E **66**, 011405 (2002).
[8] A. M. Puertas, M. Fuchs, and M. E. Cates, Phys. Rev. E **67**, 031406 (2003).
[9] F. Sciortino, P. Tartaglia, and E. Zaccarelli, Phys. Rev. Lett. **91**, 268301 (2003).
[10] G. Foffi et al., Phys. Rev. E **65**, 050802(R) (2002).
[11] T. Eckert and E. Bartsch, Phys. Rev. Lett. **89**, 125701 (2002).
[12] K. N. Pham et al., Phys. Rev. E **69**, 011503 (2004).
[13] D. A. Young and B. J. Alder, Phys. Rev. Lett. **38**, 1213 (1977).
[14] N. Osterman et al., Phys. Rev. Lett. **99**, 248301 (2007).
[15] J. Duran, *Sands, Powders, and Grains: An Introduction to the Physics of Granular Materials* (Springer, New York, 1999).
[16] J. Horbach, J. Phys.: Condens. Matter **20**, 244118 (2008).
[17] E. A. Jagla, J. Chem. Phys. **111**, 8980 (1999).
[18] T. Franosch et al., Phys. Rev. E **55**, 7153 (1997).
[19] F. J. Rogers and D. A. Young, Phys. Rev. A **30**, 999 (1984).
[20] A. Lang et al., J. Phys.: Condens. Matter **11**, 10143 (1999).
[21] M. Sperl et al., (2010), in preparation.
[22] M. J. Lighthill, *Introduction to Fourier Analysis and Generalized Functions* (Cambridge University Press, Cambridge, 1962).
[23] M. S. Wertheim, Phys. Rev. Lett. **10**, 321 (1963).
[24] C. A. Angell, E. D. Finch, and P. Bach, J. Chem. Phys. **65**, 3063 (1976).
[25] G. Foffi et al., Phys. Rev. Lett. **90**, 238301 (2003).
[26] N. V. Gribova et al., Phys. Rev. E **79**, 051202 (2009).
[27] Z. Yan et al., Phys. Rev. E **77**, 042201 (2008).
[28] N. N. Barraz, E. Salcedo, and M. C. Barbosa, J. Chem. Phys. **131**, 094504 (2009).